Collagen-based brain microvasculature model *in vitro* using three-dimensional printed template

Jeong Ah Kim,[1,2,a)] Hong Nam Kim,[1,a)] Sun-Kyoung Im,[3] Seok Chung,[2] Ji Yoon Kang,[1,4,b),c)] and Nakwon Choi[1,4,b),c)]
[1]*Center for BioMicrosystems, Brain Science Institute, Korea Institute of Science and Technology (KIST), Seoul, South Korea*
[2]*School of Mechanical Engineering, Korea University, Seoul, South Korea*
[3]*Center for Neuroscience, Brain Science Institute, Korea Institute of Science and Technology (KIST), Seoul, South Korea*
[4]*Department of Biomedical Engineering, Korea University of Science and Technology (UST), Daejeon, South Korea*

(Received 8 December 2014; accepted 30 March 2015; published online 15 April 2015)

We present an engineered three-dimensional (3D) *in vitro* brain microvasculature system embedded within the bulk of a collagen matrix. To create a hydrogel template for the functional brain microvascular structure, we fabricated an array of microchannels made of collagen I using microneedles and a 3D printed frame. By culturing mouse brain endothelial cells (bEnd.3) on the luminal surface of cylindrical collagen microchannels, we reconstructed an array of brain microvasculature *in vitro* with circular cross-sections. We characterized the barrier function of our brain microvasculature by measuring transendothelial permeability of 40 kDa fluorescein isothiocyanate-dextran (Stoke's radius of ~4.5 nm), based on an analytical model. The transendothelial permeability decreased significantly over 3 weeks of culture. We also present the disruption of the barrier function with a hyperosmotic mannitol as well as a subsequent recovery over 4 days. Our brain microvasculature model *in vitro*, consisting of system-in-hydrogel combined with the widely emerging 3D printing technique, can serve as a useful tool not only for fundamental studies associated with blood-brain barrier in physiological and pathological settings but also for pharmaceutical applications. © *2015 AIP Publishing LLC*. [http://dx.doi.org/10.1063/1.4917508]

I. INTRODUCTION

As a part of the neurovascular unit, the blood-brain barrier (BBB) is a dynamic interface controlling selective mass transfer between brain tissue and the circulatory system in the central nervous system (CNS), and such barrier properties distinguish BBB from other endothelia observed in peripheral tissues.[1] To protect the CNS from potential disease, BBB acts as a physical and chemical barrier *via* the formation of complex tight junctions between adjacent brain endothelial cells. This tight junction forces most of molecular traffic to take a transcellular route across BBB rather than a paracellular manner, and thus, the endothelium permits transport of only indispensable nutrients and oxygen while restricting the delivery of harmful and toxic compounds.[2–5] Therefore, BBB plays an important role in regulating overall transport phenomena of various small- and macro-molecules, and ultimately maintains homeostasis of the brain microenvironment. It has been also known that various cells such as pericytes, neurons, and glial cells persistently interact each other for regulating cerebral blood flow in BBB.[6–8] Because the damage or dysfunction on BBB is associated with a large number of neurological disorders

[a)]J. A. Kim and H. N. Kim contributed equally to this work.
[b)]J. Y. Kang and N. Choi contributed equally to this work.
[c)]Electronic addresses: jykang@kist.re.kr and nakwon.choi@kist.re.kr

such as neurodegenerative disease, brain tumor, and ischemia, interests in the BBB have been increasingly spanning from fundamental studies on the degradation of barrier functions to the discovery of therapeutic targets.[2,5,9]

For these reasons, various *in vitro* BBB models have been suggested for last few tens of years.[5,10–17] As a representative and early-developed *in vitro* model, the transwell system has been widely used to investigate the transport of a number of molecules including drug candidates across an endothelial cell layer.[5,16] Endothelial cells can be mono-cultured on porous polymeric membranes or co-cultured with other cell types such as astrocytes and pericytes by attaching them on either the other side of the membranes or the bottom of well plates. Due to pore sizes in sub- or micrometer scales and typical thickness ($\sim$10 μm) of commercially available membranes, brain endothelial cells have limited chances to interact with heterogeneous cell types directly by physical contacts and thus mostly rely on indirect interactions such as paracrine signaling. Although these transwell-based *in vitro* BBB models have shown great potentials attributed to their ease of use, relatively low cost, repeatability, and feasibility in high-throughput screening, they are still lack of physiologically more relevant conditions such as exposure of shear flows to endothelia, biomaterial consideration allowing for cell-cell interactions, and 3D environment of non-endothelial cells.[18]

To address such issues of the conventional BBB system *in vitro*, microfluidics-based BBB models *in vitro* have been recently developed.[17,19] These miniaturized systems have strong potential in recapitulating physiological conditions including maintenance of consistent biochemical gradients,[10] controlled fluidic shear stress, and mechanical properties of processed materials.[13] By adapting these advantages of the microfluidics-based systems, recent vascular models *in vitro* allow for culture of endothelial cells in microfluidic chip-embedded porous membrane[15,20] or a hydrogel block incorporated in miniaturized chips.[10–12] In spite of technologically substantial advances (i.e., on-chip systems), most of the studies have presented porous membranes sandwiched within polydimethylsiloxane (PDMS)-based square channels. To construct a physiologically more relevant system, Moya, *et al*. have recently developed a microchamber-based tissue culture platform. They reported that self-assembled endothelial cells and tissue spheroid embedded in a fibrin matrix were cultured for up to 40 days in a perfused condition.[21,22] Their hydrogel-based culture platform presents a great example for a co-culture platform of vasculature as well as tissue cells.

Here, we present an array of engineered 3D brain microvascular structure fabricated in the middle of a collagen I matrix. We utilized the widely emerging 3D printing technique to create a frame encasing the collagen matrix with well-defined spacing between vascular microchannels. Then, we demonstrate the formation of multiple microvessels by culturing mouse brain endothelial cells on the luminal surface of collagen microchannels. Owing to our brain microvascular structure well-defined in a system-in-hydrogel, we were able to characterize the barrier function of brain endothelia in a quantitative manner by optically monitoring interfacial transport of a fluorescently labeled molecule across our engineered brain microvasculature to the bulk of collagen hydrogel. In addition, the well-defined structure allowed for predicting transient mass transport with an analytical model that was coupled to estimate transendothelial permeability of the fluorescent molecule. To demonstrate the validity of our brain microvasculature, we disrupted the barrier function with mannitol and monitored its recovery. Finally, we discuss implications of our brain microvasculature model *in vitro* for applications and further studies.

II. MATERIALS AND METHODS

A. Fabrication of 3D printed frame

A polymeric frame was fabricated by three-dimensionally co-printing Vero White Plus-FullCure 835 resin as a main framework and poly-vinyl alcohol (PVA) as a dissolvable support material not only to encase collagen hydrogel but also to define positions of microchannels as templates for brain endothelia. The resins were co-printed using EDEN 260 V 3D printing system (Stratasys Inc.) with fiber diameter of 30 μm. The 3D printed block was submerged in

deionized (DI) water, and gently stirred for several hours to dissolve the PVA resin. Dimensions of the 3D printed frame were $50 \times 50 \times 3$ mm with a square opening (8×8 mm) at the center and those of 4 cylindrical microholes were either 235 or 360 μm in diameter (Fig. 1). It was also designed to include 2 protruding adapters into which PDMS reservoirs for culture media were connected.

B. Preparation of collagen gels

Collagen I was extracted from rat tails as described previously.[18,23–25] Lyophilized collagen was dissolved in 0.1% [v/v] acetic acid to adjust stock concentration of 15 mg/ml. The stock collagen was further diluted to final concentration of 5 mg/ml by adding $10 \times$ Dulbecco's modified Eagle's medium (DMEM, Corning), $1\times$ DMEM (Corning) and 0.5 N NaOH (Sigma-Aldrich). Every procedure should be done in ice to prevent undesired gelation before applying into the 3D printed frame. To visualize the fidelity of collagen microchannels, the stock collagen was conjugated with tetramethylrhodamine isothiocyanate (TRITC; Sigma-Aldrich) as previously described.[23] Briefly, the stock solution of collagen was mixed and incubated overnight with $3\times$ higher molar ratio of TRITC in 0.1 M sodium bicarbonate buffer, and then the reaction mixture was dialyzed to remove free TRITC for 3 days in dark. TRITC-collagen was re-dissolved in 0.1% [v/v] acetic acid to make another stock concentration of 15 mg/ml. The TRITC-collagen was processed in the same way as describe above.

C. Cell culture

Mouse brain endothelial cell line, bEnd.3, was purchased from American Type Culture Collection (ATCC) and cultured in high glucose DMEM supplemented with 10% [v/v] fetal bovine serum (FBS). Cells were maintained in a humidified CO_2 incubator at 37 °C.

D. Fabrication of engineered brain microvascular structure

An engineered brain microvascular structure was fabricated by using a 3D printed frame as a template for encasing collagen, a transparent poly (methyl methacrylate) (PMMA) plate as a top jig, and a duralumin plate with a hole as a bottom jig (Fig. 2(a)). Top and bottom jigs ($l = 5$ cm, $w = 5$ cm, $t = 3$ mm) supporting a middle layer were fabricated by micromachining PMMA and duralumin blocks, respectively. The bottom jig contained a shallow well ($25 \times 25 \times 0.2$ mm) in which a thin cover glass was placed for optical imaging of engineered brain microvasculature. All pieces for device fabrication were sterilized with 70% [v/v] ethanol and oxygen plasma. First, in order to allow for the adhesion between collagen and surfaces in

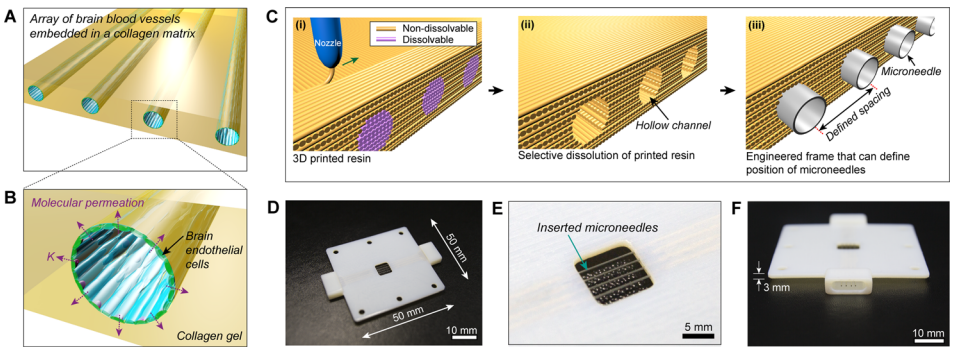

FIG. 1. (a) and (b) Conceptual illustration of our brain microvasculature system (a) and its enlarged view (b). (c)–(f) Fabrication of 3D printed frame for the construction of brain microvascular template. (c) Schematic illustration for fabrication of 3D printed frame. (i) Non-dissolvable and dissolvable resins are co-printed, and (ii) the dissolvable resin is selectively removed by submerging in DI water. (iii) Hollow channels are used for positioning microneedles. (d) A photograph of the assembled 3D printed frame and microneedles. Four microneedles with diameter of 360 μm are inserted through the hollow channels. (e) Enlarged view of collagen-encasing region (8 mm × 8 mm) of 3D printed frame. (f) Side view of 3D printed frame showing an adapter port to which a PDMS reservoir is connected.

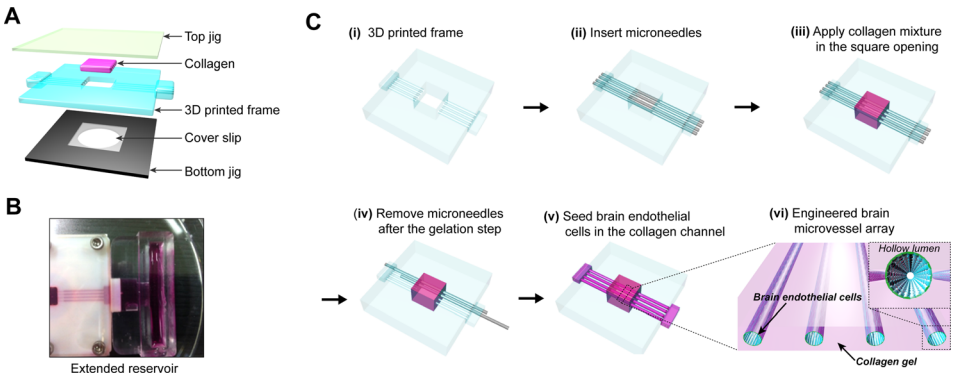

FIG. 2. (a) Exploded view of assembly components in *in vitro* brain microvasculature model. (b) Photograph showing an extended PDMS reservoir connected to collagen microchannels. (c) Fabrication steps for brain microvascular structure embedded in collagen matrix. After the insertion of microneedles into the 3D printed frame (ii), and collagen mixture is applied in the square opening of 3D printed frame (iii). After geleation, the microneedles are slowly removed from the bulk collagen (iv), leaving behind four microchannels within the collagen matrix. (v) By seeding brain endothelial cells in the collagen microchannels, array of brain microvessels embedded within collagen is formed (vi).

contact with it, inner surfaces of the square opening in the 3D printed frame and one side of a square cover glass ($25 \times 25 \times 0.2$ mm) were treated sequentially with 1% [v/v] polyethyleneimine (PEI) for 30 min and 0.1% [v/v] glutaraldehyde for 30 min. Then, the glutaraldehyde-coated surfaces were washed twice with distilled water thoroughly. Second, microneedles (outer diameter of 235 or 360 μm; Hamilton) were inserted through the cylindrical microholes in the 3D printed frame (Fig. 2(cii)). After assembling the 3D printed frame with the bottom jig, a pre-mixed collagen solution was applied slowly until just filling the square opening (8×8 mm) where the microneedles and a glutaraldehyde-coated cover glass were already positioned (Fig. 2(ciii)). Then, the top jig was covered slowly on collagen to press and confine the gel uniformly. The three layers were assembled together with sterilized stainless steel screws at corners of our device to prevent leakage. Third, collagen in the assembled device was allowed for gelation in CO_2 incubator at 37 °C for 30 min. After the gelation, the microneedles were slowly pulled out from the bulk collagen so that hollow tubular microvessels (diameter: 235 or 360 μm, length: 8 mm, interchannel spacing: 1 mm) were created within the gelated collagen (Fig. 2(civ)). Then, inner surfaces of collagen microchannels were coated with 20 μg/ml of fibronectin (Sigma-Aldrich) for 30 min to promote the adhesion of bEnd.3 cells. Fourth, a suspension of bEnd.3 cells (5×10^6 cells/ml) was loaded into the fibronectin-coated collagen microchannels, and then the device was placed in the incubator for 10 min (Fig. 2(cv)). To increase areas of initial cell adhesion, the device was quickly flipped over and incubated for another 10 min. During culture periods, a pair of extended reservoirs, fabricated separately with PDMS, was connected into the two adapters in the 3D printed frame (Fig. 2(b)). About 1.5 ml of media was applied to each PDMS reservoir and replaced every day for culture periods of up to 21 days.

E. Immunofluorescence staining

bEnd.3 cells cultured on collagen microvessels for 1, 4, 7, 14, and 21 days were fixed with 4% [v/v] paraformaldehyde for 15 min and then permeabilized with 0.1% [v/v] Triton X-100 solution for 15 min. These chemical reagents were applied into the endothelialized microchannels by hydrostatically induced laminar flow with a flow rate of ~0.1 mm/s. Mouse anti-ZO-1 antibody (Life Technologies) diluted (1:100) with a blocking solution (i.e., 1% [w/v] bovine serum albumin (BSA) in phosphate buffered saline (PBS)) was applied through microfluidic brain endothelia and incubated for 1 h. After washing microchannels by flowing PBS, bEnd.3 cells were incubated with Alexa 488-labled anti-rabbit secondary antibody (Life Technologies) for 1 h. After washing the microchannels in the same way as described above, F-actin and nuclei were stained with Phalloidin-TRITC (Sigma-Aldrich) for 1 h and 4′,6-diamidino-2-phenylindole (DAPI; Sigma-Aldrich) for 30 min, respectively. Confocal images of immunostained

bEnd.3 cells were acquired with Zeiss LSM700 laser scanning confocal microscope (Zeiss). Orthogonal projection and 3D reconstructed images were generated from Zen software (Zeiss).

F. Transendothelial permeability assay

To measure transendothelial permeability across our microfluidic brain microvasculature, 10 μM of 40 kDa fluorescein isothiocyanate (FITC)-dextran (Sigma-Aldrich) in PBS was used. Immediately after filling collagen microchannels with the FITC-dextran solution, the flow was stopped to allow for transient interfacial diffusion with an instantaneous initial condition. The temporal evolution of molecular transport was acquired by capturing sequential fluorescence images for initial 5 min with Zeiss LSM700 laser scanning confocal microscope (Zeiss). The acquired images were color-mapped and mean fluorescence intensity values across microchannels were analyzed with custom-written MATLAB (MathWorks) codes. Then, temporal profiles of the mean fluorescence intensity at 250 μm from edges of each microchannel were fitted with our analytical model to estimate the transendothelial permeability.

G. Disruption of barrier function with mannitol

0.3 M D-mannitol (Sigma-Aldrich) solution was used to transiently disrupt the barrier function of engineered brain endothelia. After the aspiration of media, 20 μl of the D-mannitol solution was introduced in a reservoir, and subsequently, the flow was stopped by balancing the height of the two reservoirs. The brain endothelia under the treatment of mannitol were incubated in 37 °C for 30 or 60 min. The transendothelial permeability of disrupted brain endothelia was measured in the same way as described above.

To observe a recovery of the permeation barrier, the transiently disrupted brain microvasculature was carefully washed with PBS for 10 min after the measurement of transendothelial permeability. Then, it was cultured additionally for 4 days in a CO_2 incubator at 37 °C. The transendothelial permeability of recovered brain endothelia (4 days after the mannitol treatment) was measured in the same way as described above.

III. RESULTS

A. Fabrication of 3D printed frame

Organs *in vivo* consist of hierarchical vascular networks not only for the efficient transport of both oxygen and essential nutrients but also for effective removal of byproducts.[26] Inspired from such vasculature *in vivo*, efforts to develop engineering tools related to tissue engineering have been more increasingly focusing on vascularized tissues *in vitro* such as tissue-on-chips[21] or transplantable tissue constructs. For the realization of vascular structures *in vitro*, it is inevitable to consider spacing (or density) between them since mass transport from the vasculature to its surroundings strongly depends on interdistance between vessel walls as well as metabolic consumption in the surrounding tissue. Effective molecular transport through hydrogels is usually valid within a few hundreds of micrometers.[27] For a systematic study on molecular transport in association with the barrier function of brain microvasculature, we created a frame to define positions of microneedles used as a removable template for the formation of cylindrical microchannels within collagen hydrogel (Fig. 1(c)). We utilized a commercially available 3D printer that co-printed non-dissolvable and dissolvable resins. Subsequent removal of the dissolvable portion by submerging in water allowed for cylindrical microholes in the middle of the frame. We confirmed shape fidelity including intended diameter of hollow microcylinders and interdistance between them. As shown in Figs. 1(d)–1(f), the four microneedles are positioned with equal spacing of 1 mm. Due to rigidity of microneedles available, combined with current resolution limits with typical 3D printers, we found that relatively large microneedles ranging from 235 to 360 μm in diameter led to high reproducibility for the creation of defect-free collagen microchannels. Including a potential possibility of utilizing our culture platform for co-cultures with brain endothelial cells on inner surfaces of microchannels and other cell types within collagen, we chose the interchannel distance of 1 mm primarily based on (1) the

resolution of 3D printing associated with the placement of microneedles and (2) reproducible removal of the microneedles without damages of the collagen structure. However, cell density as well as metabolic rates of cells seeded in abluminal space, which determines diffusion-reaction (i.e., consumption) of nutrients and oxygen,[12,28–30] should be also carefully considered, as multiple cell types will be incorporated. Note that we observed minimal swelling of the 3D printed frame when exposed to humid and warm environment. However, the swelling did not lead to the failure of operation for three weeks mostly because the rigid top and bottom jigs maintain mechanical integration throughout the experiment.

B. Construction of collagen microchannels

We chose collagen I as a scaffold matrix mainly because it allowed for great structural fidelity of microchannels as the template for brain endothelialization and served as a representative fibrous hydrogel readily allowing for cellular remodeling such as coverage towards full endothelialization. In addition, we confirmed that elastic modulus of 5 mg/ml collagen I and that of mouse hippocampus were comparable (data not shown). Although collagen IV has been reported to be an important component as basement membrane for tighter junctions between brain endothelial cells,[31,32] collagen IV as a sole scaffold material for 'brain vasculature in hydrogel' is lack of mechanical strength to retain microchannel structure as well as economic feasibility. We observed frequent failure of fabricating cylindrical microchannels (i.e., collapse of microchannels followed by the withdrawal of microneedles) embedded within composite matrices such as collagen I with fibrin, fibronectin, or Matrigel.

As shown in Figs. 2(bi)–2(bvi), we fabricated an array of cylindrical microvessel structure within 5 mg/ml of type I collagen, encased between a transparent PMMA plate and a glass cover slip assembled with a duralumin plate (Fig. 2(a)). We confirmed that the entire collagen construct was adhered onto inner sidewalls in the 3D printed frame (Figs. 3(a) and 3(b)). Figure 3(c) shows a representative bright field image after the gelation of collagen followed by the removal of microneedles. As a result, four engineered microvessels with diameter of 360 μm and inter-channel spacing of 1 mm were fabricated within the bulk collagen with smooth surfaces. The fabricated structure of collagen microchannels showed great fidelity to maintain the original geometry of circular channels with high reproducibility. When we tested lower concentration (i.e., $\leq$2.5 mg/ml) of type I collagen, the softer elastic modulus ultimately

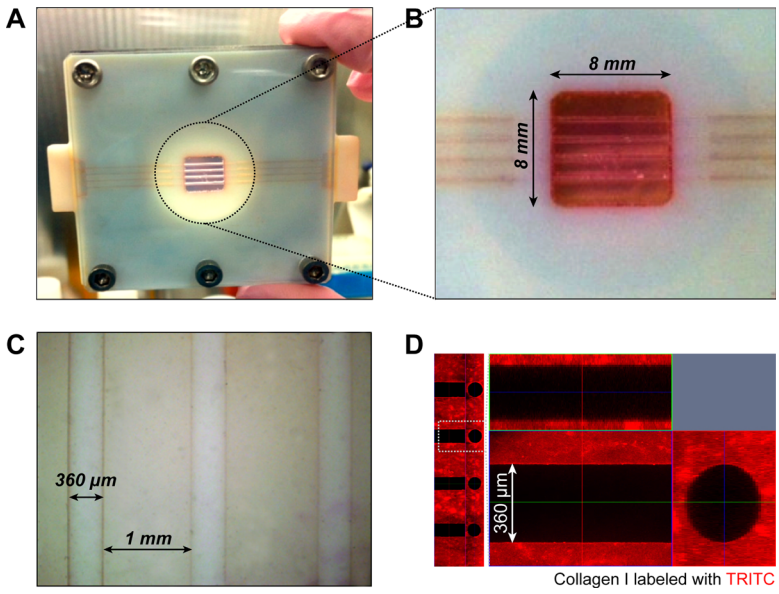

FIG. 3. (a) Photograph of our brain microvasculature system after fabrication. (b) Enlarged view of collagen microchannels. (c) Microscopic image showing multiple collagen microchannels. (d) Confocal fluorescence micrographs (*z*-stacked and orthogonal views) presenting fidelity of collagen microchannels. Collagen I was labeled with TRITC in advance.

induced undesirable collapse of channels when retracting microneedles from the solidified collagen gel (data not shown). To visualize the geometry of collagen microchannels, we utilized TRITC-labeled collagen. As shown in the top and cross-sectional views (Fig. 3(d)), four channels with defined spacing and smooth luminal surfaces were successfully fabricated.

C. Formation of engineered brain microvasculature

We used the bEnd.3 cell as a model cell type in our brain microvasculature system. For promoting of adhesion and growth of bEnd.3 on the collagen vessel, fibronectin (20 μg/ml) was coated prior to seeding cells. Compared to non-coated collagen channel, the efficiency of adhesion and growth was improved on fibronectin-coated channel (see supplementary Figs. S1A and S1B in Ref. 47). When we introduced a high density of cell suspension (i.e., 5×10^6 cells/ml) into collagen microchannels, most cells adhered onto the bottom side of the cylindrical lumen due to gravity-induced sedimentation. Considering the circular cross-section of microchannels, such seeding method in the presence of cell sedimentation might require a longer period of culture until the cells would cover the entire lumen of microchannels. It could also lead to undesirably non-uniform cell density and morphology on top and bottom sides while culture continues. Therefore, we reasoned that it would be more desirable to plate cells more uniformly at the stage of cellular attachment onto collagen microchannels.

For this purpose, we plated cells in a step-wise manner as follows. After 10 min of the introduction of a cell suspension into the microchannels, we flipped the entire device upside down. During this step, adhered cells earlier still remained attached while less adhered cells detached and settled down on the opposite side of the collagen microchannels. After another 10 min, we returned the device back as it was, resulting fairly uniform attachment of bEnd.3 cells on both top and bottom sides. This two-step plating method presented reduced time for complete formation of cell monolayer and uniform cell density and morphology, irrespective of positions. Attached cells started to spread and demonstrated distinct spindle-shaped morphology of endothelial cells. With our two-step plating method, bEnd.3 cells covered the luminal side of collagen microchannels on days 3–4, but the cells were further cultured additionally for up to three weeks towards maturation of tight junctions between the brain endothelial cells.

Our utilization of the 3D printed frame presents two advantages: (1) it served as a mechanical support during the removal of microneedles after the gelation of collagen, leading to successful fabrication of microchannels with a yield of ~90%, and (2) the adhesion between collagen and the 3D printed frame prevented the endothelialized collagen construct from being contracted over long periods of time up to 3 weeks. In case of the endothelialized collagen construct freely floated (i.e., disassembled from the 3D printed frame), we observed brain endothelial cell-induced contraction of collagen about 45% over 4 days of culture (see supplementary Figs. S1C and S1D in Ref. 47) as similarly reported.[33]

We operated our microfluidic culture with gravity-driven perfusion leading to relatively high flow rate and thus high Péclet number (Pe) to avoid depletion of nutrients and oxygen to brain endothelial cells in downstream of 8–10 mm-long microchannels.[12] Based on our calculation, Pe was $\sim 10^3$, much larger than $L/d \sim 10$, where L and d are length and diameter of a collagen microchannel, respectively. In addition, we did not observe differences between cells in upstream and those in downstream in terms of morphology, growth rate, adhesion on collagen, and formation of tight junctions for up to 3 weeks (Fig. 4).

To visualize the array of reconstructed brain microvasculature, we immunostained bEnd.3 cells on day 14. Immunofluorescence staining images clearly show the structure of engineered brain endothelia with diameter of 235 μm (Fig. 4(a)). We observed no sprouting of brain endothelial cells into the collagen gel over 3 weeks. Orthogonal views of z-stacked confocal images demonstrate a circular cross-section of our engineered brain endothelium (Fig. 4(b)).

D. Barrier function of engineered brain microvasculature: Transendothelial permeability

In physiological environment, the brain vasculature plays a key role in protection of the brain tissues by the selective transport of oxygen, glucose, and amino acids, and by the

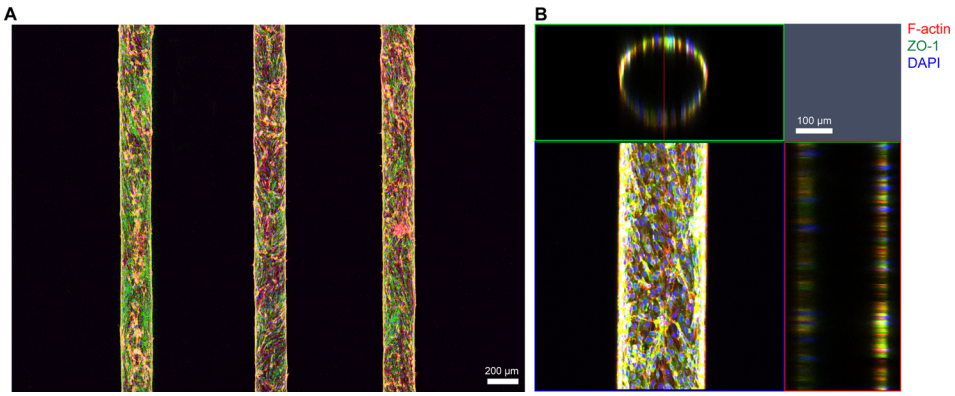

FIG. 4. Confocal fluorescence micrographs of constructed *in vitro* brain endothelia cultured for 14 days. (a) Maximum intensity projection of large-area scanned fluorescence image. (b) Orthogonal view of engineered brain microvascular structure shows hollow lumen inside. The channel shown in this figure was fabricated by using microneedles with diameter of 235 μm. Red: F-actin, green: ZO-1, and blue: nucleus.

prevention of potential toxins and pathogens as well as drugs, which is characterized with a well-known term, BBB.[34] This barrier function of BBB is originated primarily from well-developed tight junctions between brain endothelial cells. Especially, it is known that the brain capillary has 50–100 times higher expression levels of tight junction proteins among other endothelial cells existing in peripheral microvessels.[2]

To evaluate the barrier function of our engineered brain microvasculature, we measured transendothelial permeability by monitoring transient permeation of FITC-dextran from the endothelialized microchannels to the bulk of collagen hydrogel under a confocal laser scanning microscope. We loaded 10 μM of 40 kDa FITC-dextran into the channels followed by rapidly balancing volumes of the solution in both in- and outlet reservoirs. This operational condition was not only to prevent convection-mediated molecular transport but also to set up an instantaneous initial condition. We acquired fluorescence images at the same position at various time points of 0, 1, 2, 3, 4, and 5 min, with our brain endothelia cultured for 1, 2, 3, 4, 7, 14, and 21 days as well as a non-seeded control (Figs. 5(a)–5(ah)). As shown in color-mapped fluorescence micrographs as well as line profiles of longitudinally averaged fluorescence intensity (Figs. 5(a)–5(h)), leakages of 40 kDa FITC-dextran (Stoke's radius of ~4.5 nm) decreased while the coverage of bEnd.3 cells on the luminal side of collagen microchannels increased from day 1 to 4. From day 7 to 21, we observed no random leakages of the FITC-dextran across our brain microvasculature (Figs. 5(f)–5(h)). Our data show 2-stage formation of a brain endothelium. In the first stage from day 0 to 4, bEnd.3 cells continued covering the entire luminal surface, and thus, significant permeation as well as random leakages of the fluorescent molecule occurred. Although the brain endothelial cells covered nearly entire collagen microchannels on day 4, we still observed a pinhole in the left side of the endothelium (Fig. 5(e)). During the second stage from day 7 to 21, bEnd.3 cells covering collagen microchannels remained intact without pinholes while the maturation of tight junctions occurred.

E. Estimation of transendothelial permeability with analytical modeling in cylindrical brain microvasculature

To quantitatively investigate the molecular transport across the engineered brain endothelium, we formulated an analytical model in the cylindrical coordinate as similarly done in the Cartesian coordinate.[18] To do so, we made following three assumptions: (i) The fluorescent intensity was proportional to the concentration of a fluorescent solute, (ii) the molecular transport from a cylindrical microchannel to a bulk material occurred solely by diffusion without convection or hydrodynamic pressure, and (iii) there was no longitudinal variation of the concentration within the cylindrical microchannel. These assumptions were valid in our experimental system because (i) the linear proportionality maintained in low concentration ranges,[35]

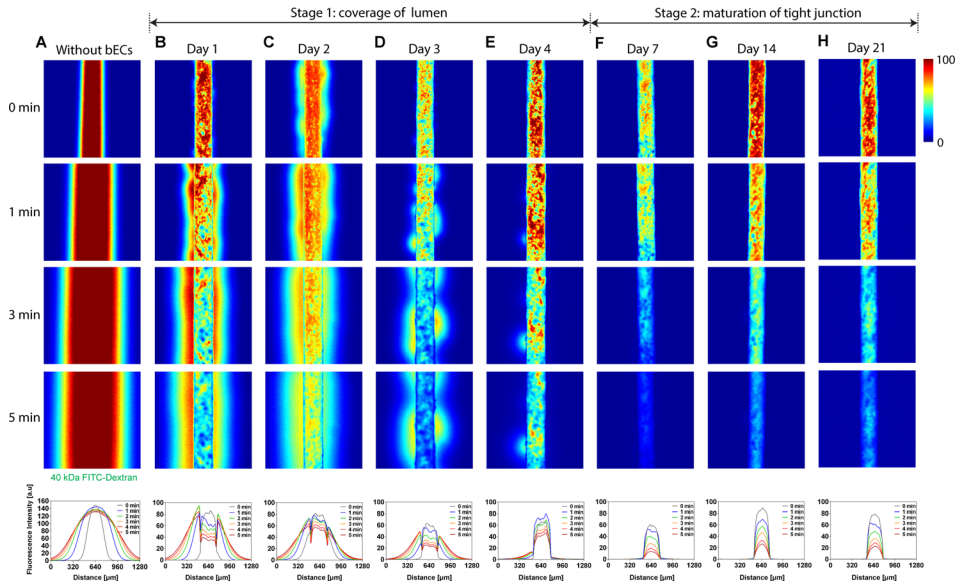

FIG. 5. Color-mapped confocal micrographs of 40 kDa FITC-dextran transported across microfluidic vasculature without bEnd.3 cells (a), on days 1 (b), 2 (c), 3 (d), 4 (e), 7 (f), 14 (g), and 21 (h). In each case, four representative images show temporal evolution of interfacial transport at 0, 1, 3, and 5 min. 40 kDa FITC-dextran leaked randomly from microfluidic brain vasculature from days 1 to 4 (stage 1: coverage of lumen), whereas no such leakage occurred from days 7 to 21 (stage 2: maturation of tight junction). Plots on bottom panel show longitudinal axis-averaged fluorescence intensity profiles corresponding to the molecular transport shown in (a)–(h). Microchannels shown here were fabricated using microneedles with diameter of 235 μm.

(ii) the macromolecule started to diffuse into the surrounding matrix under a static condition, and (iii) we loaded the FITC-dextran solution rapidly to fill the microchannels.[12]

We introduce a cylindrical coordinate system in which a fluorescent solute diffused radially into the bulk material. Then, we can set a concentration profile of the solute to be $c = c(r, t)$, diffusivity in collagen as D [cm^2/s], and transendothelial permeability across the endothelium at the microchannel-collagen interface as K [cm/s] (Fig. 6(a)). Non-dimensionalized parameters are as follows: radius $R = r/\delta$, concentration $\bar{c} = (c - c_0)/(c_i - c_0)$, del operator $\bar{\nabla} = \delta\nabla$, and time $\tau = Dt/\delta^2$.

In the bulk of collagen as a system of interest, the governing equation for a concentration distribution can be expressed as transient 1D radial diffusion (Fig. 6(b))

$$\frac{\partial \bar{c}}{\partial \tau} = \bar{\nabla}^2 \bar{c}. \tag{1}$$

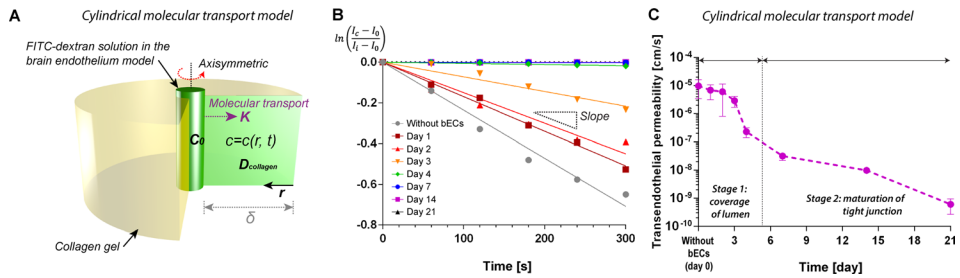

FIG. 6. Analytical modeling for transendothelial permeability in the case of microvascular structure embedded in collagen matrix. (a) Schematic illustration defining system of interest: fluorescein-labeled macromolecule (FITC-dextran) is transported radially into collagen matrix across cylindrical endothelium with permeability of K. Initial concentration of the tracing molecule in the channel is c_0, and spatio-temporal concentration profile can be defined as $c = c(r, t)$. (b) Log-linear plot of intensity profiles at distance of 250 μm from edges of the microchannels shown in Fig. 5. (c) Estimated transendothelial permeability in our brain microvasculature model. The transendothelial permeability decreases consistently over 21 days of culture. Day 0 denotes collagen channels without brain endothelial cells (bECs).

An initial condition almost equivalent to our experiment is $\bar{c}(R, 0) = 1$, and two boundary conditions at $R = 0$ and 1 are

$$\bar{\nabla}\bar{c}(0, \tau) = 0, \tag{2}$$

$$\bar{\nabla}\bar{c}(1, \tau) = -Bi\bar{c}(1, \tau), \tag{3}$$

where the Biot number is defined as

$$Bi \equiv \frac{K\delta}{D}. \tag{4}$$

With these conditions, we can obtain a general solution for the concentration distribution at position R and time τ

$$\bar{c}(R, \tau) = 2\sum_{n=1}^{\infty}\left[1 + \left(\frac{Bi}{\lambda_n}\right)^2\right]^{-1}\frac{J_1(\lambda_n)}{\{J_0(\lambda_n)\}^2}J_0(\lambda_n R)e^{-\lambda_n^2\tau}, \tag{5}$$

$$\lambda_n = B_i\frac{J_0(\lambda_n)}{J_1(\lambda_n)}. \tag{6}$$

The general solution can be approximated as follows, assuming that the first term dominates at early times:

$$\bar{c}(R, \tau) \approx 2\left[1 + \left(\frac{Bi}{\lambda_1}\right)^2\right]^{-1}\frac{J_1(\lambda_1)}{\{J_0(\lambda_1)\}^2}J_0(\lambda_1 R)e^{-\lambda_1^2\tau}, \tag{7}$$

$$\lambda_1 = B_i\frac{J_0(\lambda_1)}{J_1(\lambda_1)}. \tag{8}$$

At the distance of δ away from an edge of the cylindrical microchannel ($R = 0$), we can get

$$\ln\left(\frac{c(0, t) - c_0}{c_i - c_0}\right) = -\left(\lambda_1^2\frac{D}{\delta^2}\right)t + \ln\alpha, \tag{9}$$

where α is

$$\alpha \equiv 2\left[1 + \left(\frac{B_i}{\lambda_1}\right)^2\right]^{-1}\frac{J_1(\lambda_1)}{\{J_0(\lambda_1)\}^2}. \tag{10}$$

Thus, a linear fit of $\ln[(c(0, t) - c_0)/(c_i - c_0)]$ vs. t gives λ_1,

$$\lambda_1 = \sqrt{\frac{|\text{slope}|\delta^2}{D}}. \tag{11}$$

From the definition of Bi (Eq. (4)) and Eqs. (8) and (11), we obtain the transendothelial permeability of our engineered brain microvasculature, K as

$$K_1 = \sqrt{|\text{slope}|D}\left(\frac{J_1\left(\sqrt{\frac{|\text{slope}|\delta^2}{D}}\right)}{J_0\left(\sqrt{\frac{|\text{slope}|\delta^2}{D}}\right)}\right). \tag{12}$$

According to the linear fit of fluorescent intensity profiles, we obtained absolute values of slope for both engineered brain microvasculature and non-endothelialized case (Fig. 6(b), supplementary Fig. S3B and Table S1 in Ref. 47). With diffusivity of 40 kDa FITC-dextran in 5 mg/ml of collagen, $D = 5.5 \times 10^{-7}$ cm^2/s,[36] the transendothelial permeability without brain endothelial cells was $K_{without\ brain\ ECs} = 9.66 \times 10^{-6}$ cm/s (Fig. 6(c)). The transendothelial permeability decreased rapidly as the culture period increased. For example, on day 4, the transendothelial permeability was $K_{Day\ 4} = 2.27 \times 10^{-7}$ cm/s, which appeared to be nearly two orders of magnitude lower than that of non-endothelialized collagen channel. The transendothelial permeability continued decreasing significantly over 3 weeks with $K_{Day\ 21} = 6.03 \times 10^{-10}$ cm/s. These results suggest that the maturation of tight junctions affect the barrier function of engineered brain endothelium.

To observe the difference in tight junction formation, we immunostained bEnd.3 cells cultured for 1, 7, 14, and 21 days with ZO-1. As shown in Fig. 7 (projected view), on day 1, tight junctions barely start expressing. However, as the culture period increases from day 7 to 21, the expression level of tight junctions (ZO-1, green) becomes clearer (Fig. 7). This trend of tight junction maturation clearly correlates with the decreasing trend of transendothelial permeability (Fig. 6(c)), implying the role of tight junctions in the barrier function.

F. Disruption and recovery of barrier function

The temporal disruption of barrier function is one of major interests of pharmaceutical researchers since healthy brain vasculature prohibits the transport of drug molecules into brain tissues. To address this issue, mannitol has been widely used to open the BBB owing to its safety and efficacy.[37] We also used mannitol as a hyperosmotic model agent to disrupt the barrier function of our engineered brain endothelium. Although others used high concentrations of mannitol (e.g., 1.4–1.6 M),[37,38] we treated microfluidic brain endothelia with relatively low concentration of mannitol solution (i.e., 0.3 M), to adjust its solubility in media, for 30 or 60 min.

As shown in leakages of 40 kDa FITC-dextran (Figs. 8(a) and 8(b)), 30 min of treatment opened the barrier even with the low concentration. As expected, for the longer treatment for 60 min, the leakage increased. The transendothelial permeability of mannitol treated brain endothelia for 30 and 60 min were $K_{Mannitol\ 30\ min} = 3.90 \times 10^{-7}$ and $K_{Mannitol\ 60\ min} = 3.99 \times 10^{-6}$ cm/s, respectively. Compared with the control (day 7, non-treated, $K_{Day\ 7} = 3.18 \times 10^{-8}$), the mannitol treatment for 30 and 60 min demonstrated larger transendothelial permeability by one and two orders of magnitude.

To demonstrate the viability of our engineered brain endothelium, we also monitored a recovery of the barrier function. 4 days after the mannitol-treatment (Fig. 9(b)), the 30 min-treatment resulted in significantly lower transendothelial permeability of $K_{Recovery\ from\ 30\ min\ treament} = 2.13 \times 10^{-9}$ cm/s, which is comparable with that of brain endothelium cultured for between 7 and 14 days. However, the 60 min-treatment showed $K_{Recovery\ from\ 60\ min\ treament} = 5.29 \times 10^{-8}$ cm/s, similar to the state of day 7. These results indicate that the extent of temporal opening of brain endothelium ultimately affects the recovery of the barrier function.

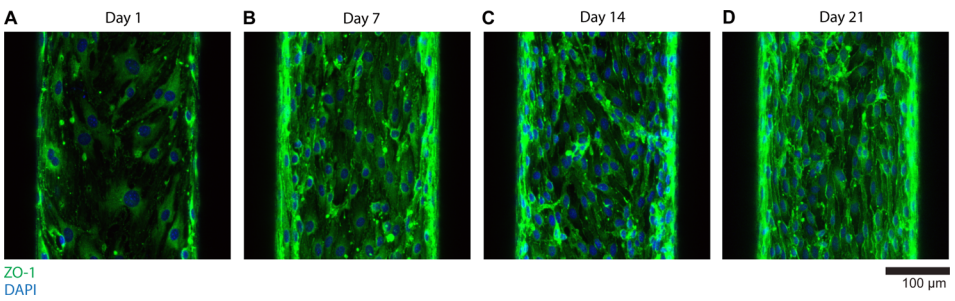

FIG. 7. Immunofluorescence imaging of tight junction (ZO-1) on days 1 (a), 7 (b), 14 (c), and 21 (d). As culture periods increase up to 21 days, the expression of tight junctions between bEnd.3 cells becomes clearer, corresponding to the trend of transendothelial permeability.

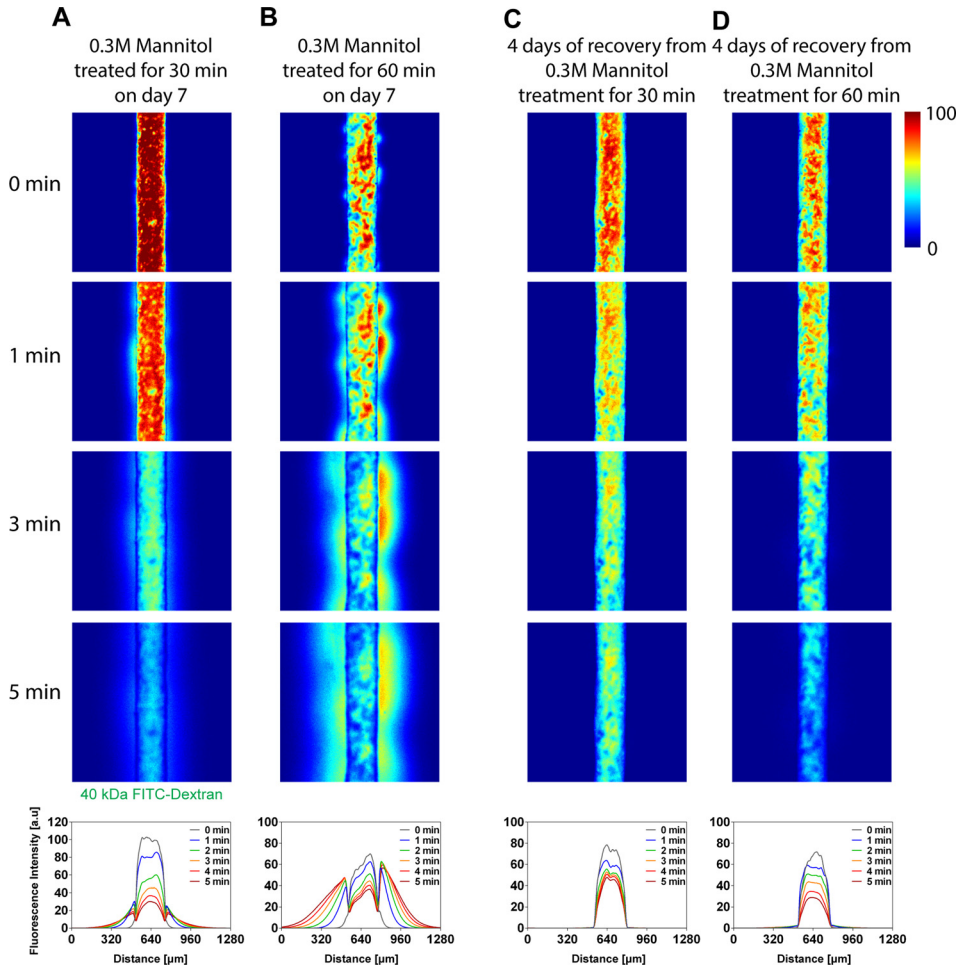

FIG. 8. Effect of hyperosmotic agent (mannitol) in the barrier function of brain endothelium. (a) and (b) Disruption of barrier function. 0.3 M mannitol solution was delivered into the engineered brain vasculature (culture time: day 7) and treated for 30 (a) and 60 (b) min, respectively. The leakage of 40 kDa FITC-dextran increased as the treatment time increased. (c) and (d) Recovery of barrier function. The mannitol-treated brain endothelia were cultured additionally for 4 days, and the transendothelial permeability assay was performed. Microchannels shown were fabricated using microneedles with diameter of 235 μm.

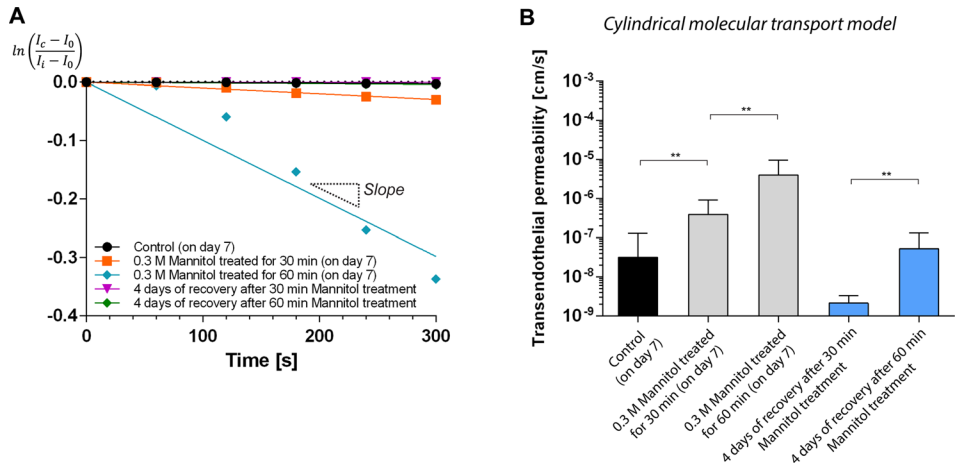

FIG. 9. (a) Log-linear plot of intensity profiles at distance of 250 μm from edges of the microchannel showin in Fig. 8. (b) Estimated transendothelial permeability in mannitol-treated endothelia (30 and 60 min) and that obtained after 4 day-recovery process (**$p < 0.01$).

IV. DISCUSSION

We have fabricated a three dimensional brain vascular structure embedded in a collagen matrix. The pre-formed geometry in the collagen matix in collaboration with coated fibronectin served as a basement membrane which supported cell adhesion and subsequent regulation of overall cell behaviors.[39] Collagen I has been a great scaffold material presenting physiologically relevant microenvironment in terms of its fibrous characteristics for cells to be able to remodel, softness, and permeability to small and macromolecules. Although PDMS, thermoplastic polymers, and glass tubes have been used to fabricate vascular structures *in vitro*, their mechanical properties (PDMS: 1–3 MPa, thermoplastic polymers: 1–2 GPa, and glass: ∼80 GPa) are much higher than those of typical tissue components *in vivo*.[40] Since the cell functions have been reportedly mediated by the mechanical properties of materials, high mechanical stiffness may exaggerate overall cell functions in an unexpected way.[41–43] In this study, we used 5 mg/ml of collagen I known to show the elastic moduli around 100 Pa (gelation at 37 °C),[44] which was far smaller compared to conventional engineering materials and even closer to that of brain *in vivo*.[45]

Towards reconstructing more physiologically relevant microenvironment where other cell types in brain such as astrocyte, pericyte, and neuron, it could be beneficial to introduce other extracellular matrix (ECM) compoments. For example, glycoprotein and proteoglycan are abundant ECM components in brain,[31] and specifically, collagen IV is known to be also abundant in basal membrane which helps expressing tight junction proteins between brain endothelial cells.[31,32] However, in our experience, collagen IV is too soft to fabricate stand-alone microstructures and relatively expensive. Collagen IV is yet more appropriate as an additive or a coating material.

It has been known that cellular microenvironments such as interstitial flow and mechanical property of gels affect the sprouting of endothelial cells (ECs) even without chemical cues such as vascular endothelial growth factor (VEGF). For example, in other 3D microfluidic model, interstitial flow and shear stress increased the chance of sprouting and migration of ECs through gel,[46] leading to focal leaks. However, in our engineered brain microvasculature model *in vitro*, bEnd.3 cells demonstrated early adhesion and spreading, and long-term viability for up to three weeks on fibronectin-coated collagen microchannels. The brain endothelial cells cover the luminal surface completely by 3–4 days, yet we observed no sprouting towards the bulk of collagen. This implies the quiescent state of endothelium, attributed to higher concentration of collagen (i.e., denser ECM fibers compared with the typical concentration of 2 mg/ml collagen).[12,46] In addition, the luminal flow stabilized endothelium, as similarly presented in Song and Munn[46] where they elucidated the effect of interstitial and luminal flows in angiogenic sprouting.

To demonstrate the applicability of co-culture of multiple cell types in our culture platform, we cultured mouse primary astrocytes within collagen with a seeding density of 10^6 cells/ml for 4 days in the presence of brain endothelialized microchannels. Astrocyte feet were sprouting (black arrow heads in supplementary Fig. S2 in Ref. 47) similarly as *in vivo*.

With our analytical model to calculate the transendothelial permeability, we have derived the spatio-temporal concentration profile of a fluorescent solute under a transient diffusion process. By applying principles of transport phenomena in the cylindrical coordinate system (i.e., *r*-direction), we obtained an analytical expression for transendothelial permeability characterized by the ratio of Bessel functions of the first kind. If we apply the in-plane (1D) diffusion model in the Cartesian coordinate, the permeability can be expressed as[18]

$$K_{cartesian} = \sqrt{|\text{slope}|D_{collagen}}\tan\left(\sqrt{\frac{|\text{slope}|\delta^2}{D_{collagen}}}\right), \tag{13}$$

where the absolute value of slope can be obtained identically to Eq. (11). From this simpler 1D diffusion model, calculated values of the permeability are 3.75×10^{-9} cm/s for the 21 days cultured brain endothelium, and 5.33×10^{-4} cm/s for non-endothelialized channel (supplementary Fig. S3C and Table S1 in Ref. 47). The transendothelial permeability values obtained from in-plane transport model were generally one order of magnitude higher compared with those

obtained from the cylindrical transport model. Such difference in transendothelial permeability was also reflected on the mannitol-treatment experiments (supplementary Fig. S4 and Table S2 in Ref. 47). In our experimental setting, the molecular transport occurred radially; therefore, the simpler 1D diffusion model was likely to overestimate the barrier function of our engineered brain microvasculature model.

Interestingly, we found that changes in diffusivity (and thus the concentration of collagen) within an order of magnitude played a very minor role in affecting K whereas interfacial transport across brain endothelial barriers over time served as a predominant factor (supplementary Fig. S5 in Ref. 47). To predict the extent of the dependence, we theoretically mapped the two parameters (i.e., D and |slope|) affecting K by setting up a few hypothetical cases based on practical ranges of diffusivity and |slope|. Note that we used a minimum value of 2×10^{-7} cm^2/s corresponding to diffusivity of 40 kDa FITC-dextran in 2.4 mg/ml of collagen and a maximum value of 6.5×10^{-7} cm^2/s corresponding to that in 45 mg/ml of collagen.[36] Also note that we varied |slope| ranging from 10^{-3} to 10^{-7} s^{-1}, corresponding to that estimated on day 1 and 21. Our scaling prediction showed that changes of diffusivity within an order of magnitude, corresponding to a practical range of collagen concentration, played a very minor role in affecting the transendothelial permeability, K, whereas interfacial transport across brain endothelial barriers over time (i.e. |slope|) served as a predominant factor in both cylindrical and in-plane transport models.

V. CONCLUSIONS

In this study, we fabricated an engineered brain vascular structure by combining the 3D printing technique and microfluidic hydrogel. These fabrication techniques allow for the recapitulation of phyiologically more relevant configurations in terms of the choice of a scaffold matrix, circular cross-section of endothelia, and the formation of tight junctions. Our engineered brain microvasculature model *in vitro* allowed for the demonstration of a time-dependent evolution of the barrier function for up to 3 weeks. In addition, the disruption of the barrier function and its functional recovery indicated the validity of our model as a useful platform towards recapitulating the brain vasculature *in vivo*. Yet, remaining challenges still include, but not limited to, the investigation of multicellular interactions between brain endothelial cells and other cells such as astrocytes and pericytes with mimicking their 3D microenvironments. Moreover, the multicellular interactions would have to be not only indirect via biochemical factors but also direct by cell-cell contacts. Although further studies still remain towards constructing fully biomimetic BBB systems to address the challenges above, we believe that our engineered platform can serve as a useful tool not only for fundamental studies associated with BBB and neurovascular unit in physiological and pathological settings but also for pharmaceutical applications.

ACKNOWLEDGMENTS

This work was supported by the KIST Institutional Program (Project Nos. 2E25474 and 2Z04110). This research was also supported by the Brain Research Program through the National Research Foundation of Korea (NRF) funded by the Ministry of Science, ICT & Future Planning (NRF-2012M3C7A1055410). This work was also supported by Basic Science Research Program through the National Research Foundation of Korea (NRF) funded by the Ministry of Science, ICT & Future Planning (NRF-2013R1A1A2060426) as well as a Korea University Grant. S. Chung was supported by BioNano Health-Guard Research Center funded by MSIP of Korea as Global Frontier Project (Grant No. H-GUARD_2014M3A6B2060524). We also thank Mr. Deogmoon Rho greatly for his efforts to help fabricate the 3D printed frame and machine other jig parts.

[1]B. Obermeier, R. Daneman, and R. M. Ransohoff, Nat. Med. **19**, 1584 (2013).
[2]N. J. Abbott, J. Anat. **200**, 523 (2002).
[3]N. J. Abbott, L. Rönnbäck, and E. Hansson, Nat. Rev. Neurosci. **7**, 41 (2006).
[4]S. H. Ma, L. A. Lepak, R. J. Hussain, W. Shain, and M. L. Shuler, Lab Chip **5**, 74 (2005).
[5]I. Wilhelm, C. Fazakas, and I. A. Krizbai, Acta Neurobiol. Exp. **71**, 113 (2011).

[6]A. Armulik, G. Genove, M. Mae, M. H. Nisancioglu, E. Wallgard, C. Niaudet, L. Q. He, J. Norlin, P. Lindblom, K. Strittmatter, B. R. Johansson, and C. Betsholtz, Nature **468**, 557 (2010).
[7]O. B. Paulson, Eur. Neuropsychopharmacol. **12**, 495 (2002).
[8]A. Prat, K. Biernacki, K. Wosik, and J. P. Antel, Glia **36**, 145 (2001).
[9]K. E. Sandoval and K. A. Witt, Neurobiol. Dis. **32**, 200 (2008).
[10]B. M. Baker, B. Trappmann, S. C. Stapleton, E. Toro, and C. S. Chen, Lab Chip **13**, 3246 (2013).
[11]M. B. Chen, S. Srigunapalan, A. R. Wheeler, and C. A. Simmons, Lab Chip **13**, 2591 (2013).
[12]N. W. Choi, M. Cabodi, B. Held, J. P. Gleghorn, L. J. Bonassar, and A. D. Stroock, Nat. Mater. **6**, 908 (2007).
[13]K. M. Chrobak, D. R. Potter, and J. Tien, Microvasc. Res. **71**, 185 (2006).
[14]L. Cucullo, M. S. McAllister, K. Kight, L. Krizanac-Bengez, M. Marroni, M. R. Mayberg, K. A. Stanness, and D. Janigro, Brain Res. **951**, 243 (2002).
[15]L. Griep, F. Wolbers, B. de Wagenaar, P. ter Braak, B. Weksler, I. A. Romero, P. Couraud, I. Vermes, A. van der Meer, and A. van den Berg, Biomed. Microdev. **15**, 145 (2013).
[16]G. Li, M. J. Simon, L. M. Cancel, Z.-D. Shi, X. Ji, J. M. Tarbell, B. Morrison III, and B. M. Fu, Ann. Biomed. Eng. **38**, 2499 (2010).
[17]B. Prabhakarpandian, M.-C. Shen, J. B. Nichols, I. R. Mills, M. Sidoryk-Wegrzynowicz, M. Aschner, and K. Pant, Lab Chip **13**, 1093 (2013).
[18]Y. Zheng, J. Chen, M. Craven, N. W. Choi, S. Totorica, A. Diaz-Santana, P. Kermani, B. Hempstead, C. Fischbach-Teschl, and J. A. López, Proc. Natl. Acad. Sci. U.S.A. **109**, 9342 (2012).
[19]R. Booth and H. Kim, Lab Chip **12**, 1784 (2012).
[20]J. W. Song, S. P. Cavnar, A. C. Walker, K. E. Luker, M. Gupta, Y. C. Tung, G. D. Luker, and S. Takayama, Plos One **4**, e5756 (2009).
[21]M. Moya, D. Tran, and S. C. George, Stem Cell Res. Ther. **4**, S15 (2013).
[22]M. L. Moya, Y. H. Hsu, A. P. Lee, C. C. W. Hughes, and S. C. George, Tissue Eng. Part C **19**, 730 (2013).
[23]V. L. Cross, Y. Zheng, N. Won Choi, S. S. Verbridge, B. A. Sutermaster, L. J. Bonassar, C. Fischbach, and A. D. Stroock, Biomaterials **31**, 8596 (2010).
[24]J. P. Morgan, P. F. Delnero, Y. Zheng, S. S. Verbridge, J. M. Chen, M. Craven, N. W. Choi, A. Diaz-Santana, P. Kermani, B. Hempstead, J. A. Lopez, T. N. Corso, C. Fischbach, and A. D. Stroock, Nat. Protoc. **8**, 1820 (2013).
[25]N. Rajan, J. Habermehl, M.-F. Coté, C. J. Doillon, and D. Mantovani, Nat. Protoc. **1**, 2753 (2007).
[26]D. Attwell, A. M. Buchan, S. Charpak, M. Lauritzen, B. A. MacVicar, and E. A. Newman, Nature **468**, 232 (2010).
[27]S. S. Verbridge, N. W. Choi, Y. Zheng, D. J. Brooks, A. D. Stroock, and C. Fischbach, Tissue Eng. Part A **16**, 2133 (2010).
[28]N. W. Choi, S. S. Verbridge, R. M. Williams, J. Chen, J. Y. Kim, R. Schmehl, C. E. Farnum, W. R. Zipfel, C. Fischbach, and A. D. Stroock, Biomaterials **33**, 2710 (2012).
[29]L. Corstorphine and M. V. Sefton, J. Tissue Eng. Regener. Med. **5**, 119 (2011).
[30]T. Kihara, J. Ito, and J. Miyake, Plos One **8**, e82382 (2013).
[31]D. Bonneh-Barkay and C. A. Wiley, Brain Pathol. **19**, 573 (2009).
[32]B. Engelhardt, J. Cereb. Blood Flow Metab. **31**, 1969 (2011).
[33]K. H. K. Wong, J. G. Truslow, and J. Tien, Biomaterials **31**, 4706 (2010).
[34]N. J. Abbott, A. A. K. Patabendige, D. E. M. Dolman, S. R. Yusof, and D. J. Begley, Neurobiol. Dis. **37**, 13 (2010).
[35]A. Sharma and S. G. Schulman, *Introduction to Fluorescence Spectroscopy* (John Wiley & Sons, 1999).
[36]S. Ramanujan, A. Pluen, T. D. McKee, E. B. Brown, Y. Boucher, and R. K. Jain, Biophys. J. **83**, 1650 (2002).
[37]M. Ikeda, A. K. Bhattacharjee, T. Kondoh, T. Nagashima, and N. Tamaki, Biochem. Biophys. Res. Commun. **291**, 669 (2002).
[38]R. C. Brown, R. D. Egleton, and T. P. Davis, Brain Res. **1014**, 221 (2004).
[39]P. D. Yurchenco, Cold Spring Harbor Perspect. Biol. **3**, a004911 (2011).
[40]H. N. Kim, D. H. Kang, M. S. Kim, A. Jiao, D. H. Kim, and K. Y. Suh, Ann. Biomed. Eng. **40**, 1339 (2012).
[41]P. Hersen and B. Ladoux, Nature **470**, 340 (2011).
[42]J. Park, H. N. Kim, D. H. Kim, A. Levchenko, and K. Y. Suh, IEEE Trans. Nanobiosci. **11**, 28 (2012).
[43]C. Yang, M. W. Tibbitt, L. Basta, and K. S. Anseth, Nat. Mater. **13**, 645 (2014).
[44]Y. L. Yang, L. M. Leone, and L. J. Kaufman, Biophys. J. **97**, 2051 (2009).
[45]A. J. Engler, S. Sen, H. L. Sweeney, and D. E. Discher, Cell **126**, 677 (2006).
[46]J. W. Song and L. L. Munn, Proc. Natl. Acad. Sci. U.S.A. **108**, 15342 (2011).
[47]See supplementary material at http://dx.doi.org/10.1063/1.4917508 for supplementary method, figures, and tables.